Key Points:
- An electron-scale current sheet was observed in the near-Earth tail
- The electron-scale current sheet was observed without any bursty reconnection signatures
- The Hall electric field drift of electrons accounts for the formation of the electron-scale current sheet

Correspondence to:
R. Wang and Q. Lu,
rswan@ustc.edu.cn;
qmlu@ustc.edu.cn

An Electron-Scale Current Sheet Without Bursty Reconnection Signatures Observed in the Near-Earth Tail

Rongsheng Wang[1] (iD)**, Quanming Lu[1]** (iD)**, Rumi Nakamura[2], Wolfgang Baumjohann[2]** (iD)**, Can Huang[1], Christopher T. Russell[3]** (iD)**, J. L. Burch[4]** (iD)**, Craig J. Pollock[5]** (iD)**, Dan Gershman[5]** (iD)**, R. E. Ergun[6]** (iD)**, Shui Wang[1], P. A. Lindqvist[7]** (iD)**, and Barbara Giles[5]** (iD)

[1]CAS Key Laboratory of Geospace Environment, Department of Geophysics and Planetary Science, University of Science and Technology of China, Hefei, China, [2]Space Research Institute, Austrian Academy of Sciences, Graz, Austria, [3]Earth Planetary and Space Sciences, University of California, Los Angeles, CA, USA, [4]Southwest Research Institute, San Antonio, TX, USA, [5]NASA, Goddard Space Flight Center, Greenbelt, MD, USA, [6]Department of Astrophysical and Planetary Sciences, University of Colorado Boulder, Boulder, CO, USA, [7]School of Electrical Engineering, Royal Institute of Technology, Stockholm, Sweden

Abstract Observations of a current sheet as thin as the electron scale are extremely rare in the near-Earth magnetotail. By measurement from the novel Magnetospheric Multiscale mission in the near-Earth magnetotail, we identified such an electron-scale current sheet and determined its detailed properties. The electron current sheet was bifurcated, with a half-thickness of nine electron inertial lengths, and was sandwiched between the Hall field. Because of the strong Hall electric field, the super-Alfvénic electron bulk flows were created mainly by the electric field drift, leading to the generation of the strong electron current. Inevitably, a bifurcated current sheet was formed since the Hall electric field was close to zero at the center of the current sheet. Inside the electron current sheet, the electrons were significantly heated while the ion temperature showed no change. The ions kept moving at a low speed, which was not affected by this electron current sheet. The energy dissipation was negligible inside the current sheet. The observations indicate that a thin current sheet, even as thin as electron scale, is not the sufficient condition for triggering bursty reconnection.

Plain Language Summary Magnetic reconnection plays a key role for many explosive phenomena in space, astrophysical, and laboratorial plasmas. It is widely accepted that reconnection will be triggered once the current sheet thins down to ion scale. In this letter, however, an electron-scale current sheet, much thinner than ion scale, was observed without any bursty reconnection signatures. The observations indicate that a thin current sheet, even as thin as electron scale, is not the sufficient condition for triggering reconnection.

1. Introduction

The current sheet in the equatorial plane of the magnetotail plays a key role for the temporal storage of the energy, mass, and magnetic fluxes from the solar wind (Baumjohann et al., 2007; Ness, 1965; Russell & Mcpherron, 1973). It is now well known that instabilities can occur inside this magnetotail current sheet and lead to magnetic reconnection and current disruption. Thereby, the stored magnetic energy is released and transferred into the near-Earth tail and ionosphere, which subsequently causes a global disturbance of the Earth's magnetic field, for example, a substorm. Many efforts have been devoted to examine dynamics and properties of the magnetotail current sheet (e.g., Asano et al., 2005; Baumjohann et al., 2007; Nakamura, Baumjohann, Asano, et al., 2006; Nakamura, Baumjohann, Runov, & Asano, 2006; Runov et al., 2005; Shen et al., 2008; Speiser, 1967; Wang et al., 2012; Zelenyi et al., 2016; Zheng et al., 2012). The observations show that the current sheet deviates from a Harris current sheet in most situations and often is bifurcated (Asano et al., 2005; Nakamura, Baumjohann, Asano, et al., 2006; Phan et al., 2006; Runov et al., 2003; Runov et al., 2006; Wang et al., 2012) and rapidly flaps up and down (Asano et al., 2005; Sergeev et al., 2003; Sergeev et al., 2004; Zhang et al., 2002).

A thin current sheet of several ion inertial lengths has been frequently observed inside this magnetotail current sheet in recent years (Baumjohann et al., 2007; Nakamura, Baumjohann, Runov, & Asano, 2006; Zelenyi et al., 2016), thanks especially to the four-point Cluster measurements. In general, the thin current

sheet is embedded in a much broader plasma sheet (Asano et al., 2005; Nakamura, Baumjohann, Runov, & Asano, 2006; Petrukovich et al., 2011), and the current within such a thin current sheet is mainly carried by electrons (Artemyev et al., 2017; Baumjohann et al., 2007; Petrukovich et al., 2011; Shen et al., 2008). The closest separation of Cluster was ~250 km, close to ion inertial length. A thinner current sheet below ion scale cannot accurately be explored by the Cluster measurements. Furthermore, it remains underdetermined whether thin current sheets below ion scale can be continuously stable, since theories and simulations predict that magnetic reconnection will be triggered once the current sheet thins down to one ion inertial length (Birn & Hesse, 2001; Liu et al., 2014; Lu et al., 2013; Pritchett & Coroniti, 1995; Schindler & Birn, 2002; Sitnov et al., 2000).

In this letter, we report on an electron current sheet (abbreviated to ECS) with a half-thickness of nine electron inertial lengths. The ECS is vertical to the equatorial plane due to the flapping motion, and its current is predominantly carried by electrons and ions play little role for the total current. The signatures of the Hall effect are evident in the vicinity of the ECS.

2. Database and Observation

The Magnetospheric Multiscale (MMS) mission consists of four satellites equipped with identical instruments and began to explore the magnetotail current sheet in May of 2017. The magnetic field is sampled at 128/s (Russell et al., 2016), and the electric field is sampled at 8192/s (Ergun et al., 2016; Lindqvist et al., 2016). The time resolutions for electrons and ions obtained from the fast plasma experiment (Pollock et al., 2016) are 30 and 150 ms, respectively. At ~20:24:07 UT on 17 June 2017, MMS passed through the current sheet from the southern hemisphere to the northern hemisphere at $[-19.4, -10.4, 5.5]$ R_e in the Geocentric Solar Ecliptic (GSE) coordinate system. Since the MMS separation was less than 30 km at that time, the observations at all four satellites were almost the same and thereby only the data at mms4 were used in this letter. An overview of this crossing is shown in Figure 1 in the local current system with $L = [0.9477, 0.3012, -0.1054]$, $M = [-0.0873, -0.0729, -0.9935]$, and $N = [-0.3067, 0.9508, -0.0428]$ relative to GSE coordinates. The local current system was obtained from the minimum variance analysis (Sonnerup & Scheible, 1998) performed to the magnetic field during 20:23:30–20:24:30 UT at mms4. The normal direction of the current sheet was mainly along the y direction of the GSE coordinate system; that is, the current sheet was vertical to the equatorial plane. The timing method (Schwartz, 1998) was also used to estimate the normal direction of the current sheet (shown later), and the result was consistent with the minimum variance analysis result. Additionally, the result of the MDD method (Shi et al., 2005) shows that the observed current sheet had a planar structure. Figure 2a shows a schematic for this crossing in the GSE coordinates.

During 20:24:00–20:24:15 UT, MMS crossed the magnetotail current sheet (B_L evolved from ~-10 to ~15 nT, Figure 1b) and entered into its center ($|B|$ ~0 nT) at ~20:24:07 UT. The most striking feature in this crossing were the intense electron bulk flows (Figure 1d) detected around the current sheet center between 20:24:05 and 20:24:09 UT. These bulk flows were coincided with the appearance of B_M, which was negative (down to -3 nT) below the current sheet ($B_L < 0$) and became positive (up to 3 nT) above the current sheet ($B_L > 0$). The strongest electron flows were observed in the M direction. v_{eM} was always directed to the $-M$ direction and decreased to $-2,500$ km/s, ~5.4 V_A, where $V_A \approx 460$ km/s is the Alfvén speed based on $N = 0.5$ cm^{-3} and $|B| = 15$ nT. v_{eL} was positive (~12,00 km/s) near the current sheet center (B_L~0) and sandwiched between the weakly negative flows (v_{eL}~ -500 km/s) at both sides of the current sheet (20:24:05–20:24:06.2 UT and 20:24:07.8–20:24:08.5 UT). In other words, the electrons were streaming earthward near the ECS's center and tailward in the outer edges of the Hall magnetic field regions, as illustrated in Figure 2b. The speed of the ion bulk flows were less than 200 km/s in this crossing. The ions mainly flowed tailward ($V_{iL} \approx -100$ km/s) as well as dawnward ($V_{iN} \approx -50$km/s) and seemingly were not associated with the ECS (Figure 1c).

The current density ($\mathbf{J} = qN(\mathbf{V}_i - \mathbf{V}_e)$, where q is the elementary charge, N is the electron density, and $\mathbf{V}_i$ and $\mathbf{V}_e$ are the ion and electron flows, respectively) is shown in Figure 1e. The current density peaked at 240 nA/m^2 and was primarily in the M direction, except at the current sheet center, where j_L and j_M were comparable. The black dot traces in Figure 1e represent the electron current density ($\mathbf{J} = -qN\mathbf{V}_e$) and are superimposed on the three components of the current density ($\mathbf{J} = qN(\mathbf{V}_i - \mathbf{V}_e)$). It means that the current was mainly carried by electrons and that ions played a negligible role. Since the four satellites crossed the current sheet one after another, the timing method was performed to the $B_L = 0$ point to estimate the normal direction and speed of
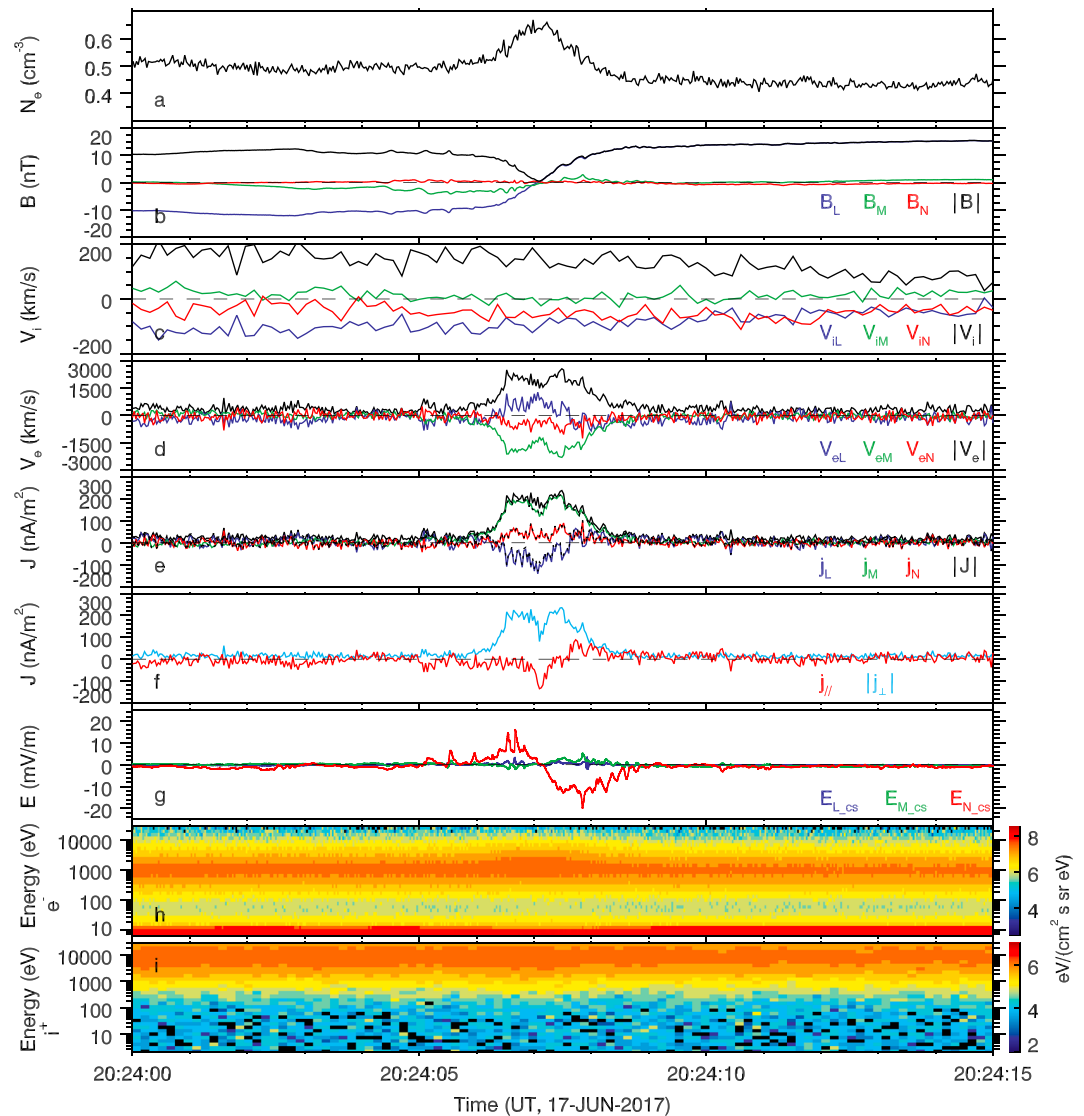
AGU
100
ADVANCING EARTH
AND SPACE SCIENCE

Geophysical Research Letters

10.1002/2017GL076330

Figure 1. An overview of the electron current sheet in the local current system at Magnetospheric Multiscale 4. (a) Electron number density, (b) three components and magnitude of the magnetic field, (c) the proton bulk flows in the three directions and the speed, (d) the electron bulk flows in the three directions and the speed, and (e) the current density $\mathbf{J} = qN(\mathbf{V}_i - \mathbf{V}_e)$ in three directions and the total current density. The black dotted lines denote the electron current density $\mathbf{J} = -qN\mathbf{V}_e$, (f) the current density in the parallel direction and the magnitude of the perpendicular current density, (g) three components of electric field in the frame of the whole magnetic structure, and (h and i) electron and ion energy spectrum.

the current sheet. The speed was 67 km/s along [0.069, 0.193, 0.979] with respect to the LMN coordinates. The duration for the ECS was ~2.0 s (~20:24:06.3 to ~20:24:08.3 UT). Thus, the half thickness of the ECS was estimated to be (67 km/s × 2.0 s)/2 ≈ 67 km ≈ 9.0 d_e, where d_e is the electron inertial length. A clear dip of the total current density was observed just at the center point ($|B| \sim 0$), and a similar dip was also observed in $|j_\perp|$ which dominated the current (Figure 1f). The decrease of the current density in the center indicates that the current sheet was bifurcated and the bifurcation mainly occurred in the perpendicular component. Figure 1g shows three components of the electric field in the frame of the current sheet. E_{N_CS} was positive below the current sheet and became negative above the current sheet. In other words, the electric field was directed to the current sheet center at both sides of the current sheet.

Based on the observations above, a schematic illustration for the current sheet is displayed in Figure 2b. MMS directly crossed the current sheet in the N direction and detected intense electron flows in the $-M$ direction,
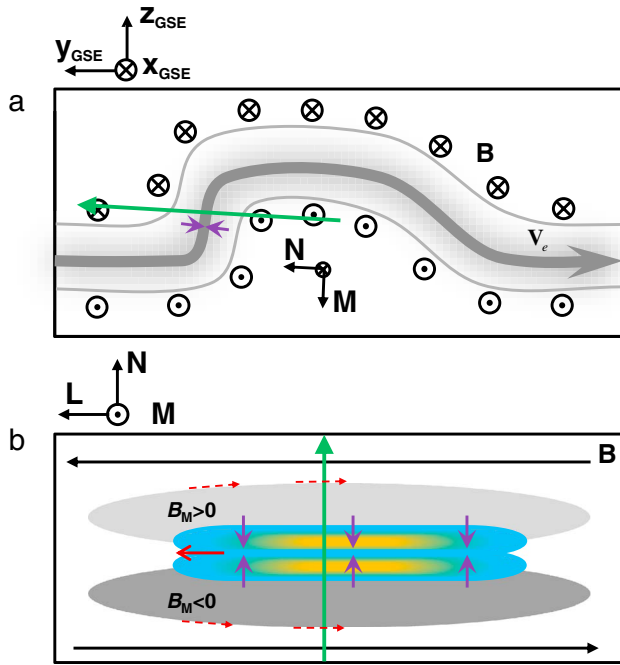
Figure 2. (a) A schematic for the magnetotail current sheet in the Geocentric Solar Ecliptic (GSE) coordinates. The circles with a dot and a cross represent magnetic field antiparallel and parallel to x axis in the GSE coordinates, respectively. The shadow region denotes the electron current sheet, and the green arrow means the Magnetospheric Multiscale trajectory relative to the current sheet. (b) The structure of the electron current sheet. The dashed and solid red arrows represent the inflowing and outflowing electron flows, respectively. The region in pale blue means the electron flows in the $-M$ direction, and the yellow regions are the enhancement regions of these electron flows. The purple arrows denote the Hall electric field. The shadow regions exhibit the Hall magnetic field regions within the current sheet.

indicated by the pale bule area in Figure 2b. The bifurcated electron flows and the resulting current (the yellow regions) were clear in the $-M$ direction. On the other hand, the electron flows in the $L - N$ plane constituted two current loops and resulted in two parts of the out-of-plane magnetic field component, namely, the negative (positive) B_M below (above) the current sheet. Furthermore, the electric field pointing to the neutral sheet was measured at both sides of the current sheet. The measured electron current loops are in agreement with the Hall electron current system (Sonnerup, 1979; Terasawa, 1983; Ma & Bhattacharjee, 1998; Wang, Bhattacharjee, & Ma, 2000; Nagai et al., 2001; Fu, Lu, & Wang, 2006; Lu et al., 2010; Wang et al., 2010). The observed bipolar E_{N_CS} as well as the bipolar magnetic field B_M are consistent with the Hall electric and magnetic fields; that is, the Hall effect was clear in the current sheet. However, only low-speed ion flows were observed and bursty bulk flows were never observed there.

Figure 3 shows electron and ion temperatures, energy dissipation in the electron frame, and electron pitch angle distribution in the same time interval as Figure 1. Again, the ion temperature both in the parallel and perpendicular directions did not show any modification in the whole crossing (Figure 3c) and remained nearly constant at ~4 keV. In contrast, the electrons were significantly heated within the intense electron flows (20:24:05–20:24:09 UT, Figure 3d). The parallel electron temperature significantly increased roughly at the weakly tailward electron flows, which was observed at the boundaries of the plasma sheet (20:24:05–20:24:06.5 UT and 20:24:07.3–20:24:09 UT) and was slightly enhanced at the ECS center. Overall, $T_{e//}$ shows the shape of a capital "M" and the dip in the middle corresponded to the ECS center. In contrast, $T_{e\perp}$ increased merely within the ECS and peaked at its center. Thus, at the ECS center, the parallel and perpendicular electron temperatures were nearly equal while, in the regions away from the center, the para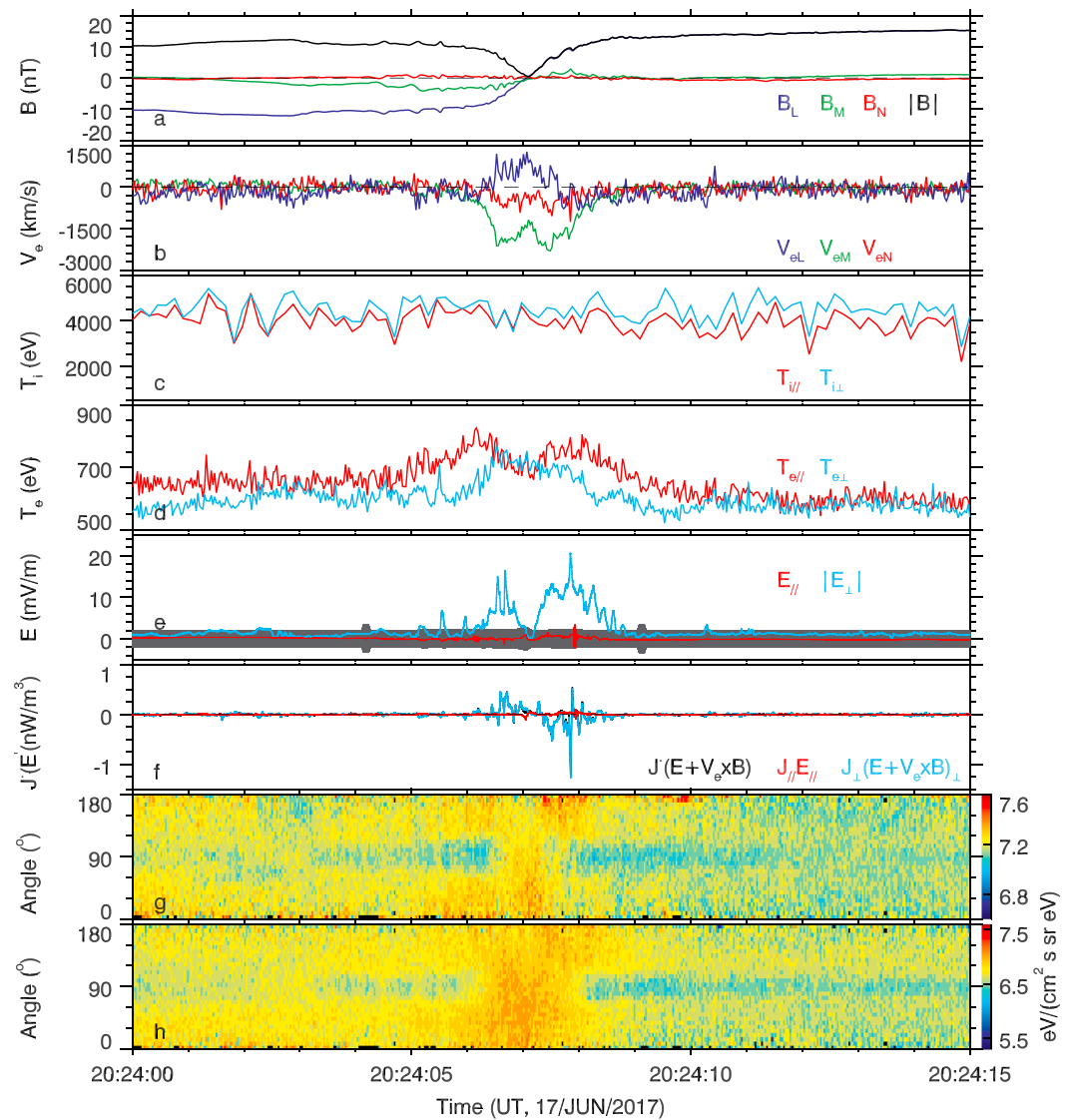llel electron temperature was larger than the perpendicular temperature. The electron pitch angle distributions at the energy levels from 200 eV to 2 keV and from 2 keV to 27 keV are shown in Figures 3g and 3h, respectively. For the electrons at the energies from 200 eV to 2 keV, the electron fluxes was significantly enhanced at ~0° before 20:24:06 UT and at ~180° after 20:24:08 UT (Figure 3g). In the energy level of 2–27 keV, the electrons exhibited a bi-streaming distribution in most regions and an isotropic distribution near the ECS center (Figure 3h).

The parallel and perpendicular electric fields are displayed in Figure 3e. In the ECS, the electric field was as strong as 20 mV/m, mostly in the perpendicular component. The high-frequent fluctuations of $E_{//}$ were found within the current sheet but away from its center, which can be seen more clearly in Figure 4a (the red traces). The most intense $E_{//}$ fluctuations were observed at ~20:24:08 UT, corresponding to the outer boundary of the Hall magnetic field. Inside the ECS, the energy dissipation was insignificant on average (Figure 3f), in comparison with those near the electron diffusion region (Burch et al., 2016; Wang et al., 2017) and the coalescence point of two flux ropes (Wang et al., 2016). The black curve representing the total energy dissipation ($\mathbf{J} \cdot (\mathbf{E} + \mathbf{V}_e \times \mathbf{B})$) was overlaid by the blue curve of the perpendicular component ($\mathbf{J}_\perp \cdot (\mathbf{E} + \mathbf{V}_e \times \mathbf{B})_\perp$), which indicates that the energy dissipation ($\mathbf{J} \cdot (\mathbf{E} + \mathbf{V}_e \times \mathbf{B})$) might mainly come from the perpendicular component ($\mathbf{J}_\perp \cdot (\mathbf{E} + \mathbf{V}_e \times \mathbf{B})_\perp$). The parallel energy dissipation ($\mathbf{J}_{//} \cdot (\mathbf{E} + \mathbf{V}_e \times \mathbf{B})_{//}$) was zero on average. Since the electrons were mainly frozen-in the magnetic field, which was addressed below, the large variation of $\mathbf{J}_\perp \cdot (\mathbf{E} + \mathbf{V}_e \times \mathbf{B})_\perp$ could come from the oscillation of the electric field, or the measurement errors, or the errors due to the different sampled rates between electric field and the plasma moment data.

The electric field was primarily in the y component of the Despun, Sunpointing L-momentum vector coordinates where the electric field was measured. So $E_{\perp y}$, $-(\mathbf{V}_i \times \mathbf{B})_y$, and $-(\mathbf{V}_e \times \mathbf{B})_y$ are shown in Figure 4b. $-(\mathbf{V}_i \times \mathbf{B})_y$ always deviated from the measured electric field $E_{\perp y}$, while $-(\mathbf{V}_e \times \mathbf{B})_y$ and $E_{\perp y}$ matched quite well,

Figure 3. (a) Three components and magnitude of the magnetic field; (b) the electron bulk flows in the three directions and the speed; (c and d) the ion and electron temperature in the parallel and perpendicular directions; (e) the parallel and perpendicular electric field, with the errors in gray; (f) the total energy dissipation and its parallel as well as perpendicular components; (g and h) electron pitch angle distributions in the middle-energy and high-energy levels, respectively. The time interval is the same to Figure 3.

except in some localized regions. It appears that ions were no longer frozen in the magnetic field, whereas electrons were still coupled with the magnetic field inside the ECS. Figure 4c shows the electric field drift velocity $\frac{\mathbf{E}_{CS} \times \mathbf{B}}{\mathbf{B}^2}$ in the L (blue) and M (green) directions and superposes the electron perpendicular velocity ($\frac{\mathbf{B} \times (\mathbf{V}_e \times \mathbf{B})}{\mathbf{B}^2}$) also in the L (pale blue) and M (pale green) directions, where $\mathbf{E}_{CS}$ is the electric field in the frame of the current sheet. The electric field drift velocity was in good agreement with the measured electron velocity, except at the ECS center where B was close to 0. So the $\frac{\mathbf{E}_{CS} \times \mathbf{B}}{\mathbf{B}^2}$ could be overestimated near the ECS center, which could be a reason for the difference. Based on the observations above, we concluded that the super-Alfvénic electron velocity was primarily formed by the electric field ($\mathbf{E} \times \mathbf{B}$) drift.

3. Discussion and Summary

The Hall effect was crucial to the dynamics of the current sheet, while the current sheet thickness decreased to ion inertial length. Inside the electron-scale current sheet, ions were no longer coupled with the magnetic
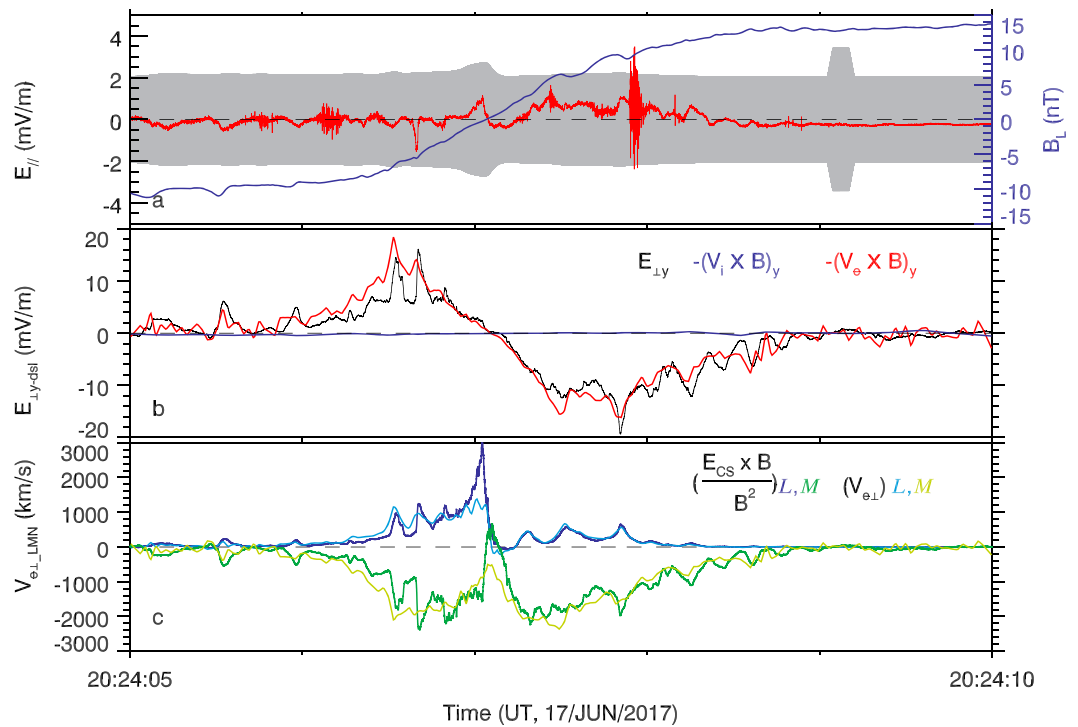
Figure 4. (a) The parallel electric field $E_{//}$ and B_L; (b) the measured electric field, $\mathbf{E}_{\perp y}$, $-(\mathbf{V}_i \times \mathbf{B})_y$, and $-(\mathbf{V}_e \times \mathbf{B})_y$ in the Despun, Sunpointing L-momentum vector coordinates; (c) electric field drift velocity in the L (in blue) and M (in green) direction and the measured electron velocity in the same directions ($\mathbf{V}_{e\perp, L}$ in pale blue, $\mathbf{V}_{e\perp, M}$ in pale green).

field lines and only the electrons remained frozen in the magnetic field lines. As a result, the Hall electric and magnetic field were produced within the current sheet. The frozen-in electrons experienced the electric field drift ($\mathbf{E} \times \mathbf{B}$) and created the electron bulk flows in the out-of-plane direction ($v_{eM} \approx -E_N \cdot B_L$). Since the values of E_N and B_L diminished at the center of the current sheet, the $|v_{eM}|$ values dropped, as did j_M and $|J|$. This explains the dips in j_M and $|J|$ at the current sheet center, namely, the bifurcation of the current sheet. In addition, the electric field drift velocity of the electrons in the L direction generated the observed v_{eL} in the ECS center. The low-speed electron flows were observed during 20:24:05.0–20:24:06.2 UT ($B_L \sim -10$ nT) below the current sheet and during 20:24:07.6–20:24:08.5 UT ($B_L \sim 10$ nT) above the current sheet, consistent with the so-called Hall electron flows (e.g., Nagai et al., 2001). They were mainly streaming along the magnetic field lines (Figures 1b and 1d), and the formation mechanism was totally different from the intense electron flows at the ECS center.

Bifurcated current sheets are frequently observed in the magnetotail (e.g., Asano et al., 2005; Nakamura, Baumjohann, Asano, et al., 2006; Runov et al., 2003; Runov et al., 2006; Wang et al., 2012) and simulated by computer (Karimabadi, Daughton, & Quest, 2005). Commonly, it is attributed to the current sheets with a plateau in B_L during reconnection (e.g., Karimabadi et al., 2005; Phan et al., 2006). In this event, the bifurcated ECS was mainly produced by the Hall electric field. The ECSs are often associated with the electron diffusion region and the separatrices during magnetic reconnection (Baumjohann et al., 2007; Burch et al., 2016; Ji et al., 2008; Nakamura, Baumjohann, Runov, & Asano, 2006; Phan et al., 2016; Wang et al., 2017). However, only low-speed ion bulk flows were observed in this ECS. Two minutes later, MMS crossed the plasma sheet again and did not observe any high speed ion flows (not shown). Therefore, this ECS was not directly related to the bursty bulk flows which were commonly regarded as the distinct signature of bursty reconnection. We conclude that this ECS was observed without any bursty reconnection signatures. The reason for the absence of the bursty reconnection in this event is still unclear. One potential reason is the electron temperature anisotropy. The ratio of $T_{e\perp}/T_{e//}$ was basically in the range of 0.8–1.0 during this event (Figure 3d). Thus, the equation $\left(1 - \frac{T_{e\perp}}{T_{e//}}\right) > \rho_e/L$ (where ρ_e is electron gyroradius and L is the half-thickness of the current sheet) was valid inside the plasma sheet, which is known to linearly stabilize the linear tearing instability

(Forslund, 1968; Laval & Pellat, 1968). On the other hand, the plasma β was high (~5) in this plasma sheet. So even if the reconnection was occurring in this ECS, it was still a high beta reconnection and did not extend to the lobe region. This is another explanation for the absence of the bursty reconnection. If so how long time the bursty reconnection would be triggered after the ECS was created is still unclear. Since the electrons drifted away from the X-line, much more electrons above and below the ECS would gather in the ECS. Namely, the high beta reconnection would extend toward the lobe region where the beta was less than 0.01. Under the condition of the low beta regime, the bursty reconnection is easily initiated (Phan et al., 2010). Thus, we speculated that the bursty reconnection was eventually triggered as the high-beta reconnection expanded into the region with a low beta.

According to the MMS measurements at the magnetopause (Wang et al., 2017), the thickness of the quadrants of the Hall magnetic field can be compressed to be a few electron inertial lengths near the reconnection X-line. In this magnetotail event, the thicknesses of the detected two Hall quadrants were estimated. The durations for the two quadrants below and above the current sheet were 1.5 and 0.7 s, respectively. Then, their individual thicknesses were 13.4 d_e and 6.3 d_e, which further confirm the previous observations (Wang et al., 2017). A background guide field $B_M \sim -1$ nT was measured in this current sheet (Figure 1b), which could account for the asymmetric distribution of the electric field at both sides of the current sheet (Figures 1g and 3e) (e.g., Wang et al., 2012).

In conclusion, an ECS was observed in the magnetotail plasma sheet, and its half-thickness was only ~9 d_e. This ECS was sandwiched between the Hall electric and magnetic field, but without any corresponding ion bursty bulk flows. It indicates that no bursty reconnection was occurring within the current sheet. This intense current of the current sheet was primarily due to the electric field drift of the electrons.

References

Artemyev, A. V., Angelopoulos, V., Liu, J., & Runov, A. (2017). Electron currents supporting the near-Earth magnetotail during current sheet thinning. *Geophysical Research Letters*, *44*, 5–11. https://doi.org/10.1002/2016GL072011

Asano, Y., Nakamura, R., Baumjohann, W., Runov, A., Voros, Z., Volwerk, M., et al. (2005). How typical are atypical current sheets? *Geophysical Research Letters*, *32*, L03108. https://doi.org/10.1029/2004GL021834

Baumjohann, W., Roux, A., le Contel, O., Nakamura, R., Birn, J., Hoshino, M., et al. (2007). Dynamics of thin current sheets: Cluster observations. *Annales de Geophysique*, *25*(6), 1365–1389. https://doi.org/10.5194/angeo-25-1365-2007

Birn, J., & Hesse, M. (2001). Geospace Environment Modeling (GEM) magnetic reconnection challenge: Resistive tearing, anisotropic pressure and Hall effects. *Journal of Geophysical Research*, *106*(A3), 3737–3750. https://doi.org/10.1029/1999JA001001

Burch, J. L., Torbert, R. B., Phan, T. D., Chen, L. J., Moore, T. E., Ergun, R. E., et al. (2016). Electron-scale measurments of magnetic reconnection in space. *Science*, *352*(6290), aaf2939. https://doi.org/10.1126/science.aaf2939

Ergun, R. E., Tucker, S., Westfall, J., Goodrich, K. A., Malaspina, D. M., Summers, D., et al. (2016). The axial double probe and fields signal processing for the MMS mission. *Space Science Reviews*, *199*(1–4), 167–188. https://doi.org/10.1007/s11214-014-0115-x

Forslund, D. W. (1968). A model of the plasma sheet in the Earth's magnetosphere, (PhD thesis). Princeton, NJ: Princeton University.

Fu, X. R., Lu, Q. M., & Wang, S. (2006). The process of electron acceleration during collisionless magnetic reconnection. *Phys. Plasmas*, *13*(1), 012309. https://doi.org/10.1063/1.2164808

Ji, H., Ren, Y., Yamada, M., Dorfman, S., Daughton, W., & Gerhardt, S. P. (2008). New insights into dissipation in the electron layer during magnetic reconnection. *Geophysical Research Letters*, *35*, L13106. https://doi.org/10.1029/2008GL034538

Karimabadi, H., Daughton, W., & Quest, K. B. (2005). Antiparallel versus component merging at the magnetopause: Current bifurcation and intermittent reconnection. *Journal of Geophysical Research*, *110*, A03213. https://doi.org/10.1029/2004JA010750

Laval, G., & Pellat, R. (1968). Stability of the plane neutral sheet for oblique propagation and anisotropic temperature. In K. Schindler (Ed.), *Proceedings of the ESRIN study group* (p. 5). Neuilly-sur_Seine, France: Eur. Space Res. Org.

Lindqvist, P. A., Olsson, G., Torbert, R. B., King, B., Granoff, M., Rau, D., et al. (2016). The spin-plane double probe electric field instrument for MMS. *Space Science Reviews*, *199*(1–4), 137–165.

Liu, Y. H., Birn, J., Daughton, W., Hesse, M., & Schindler, K. (2014). Onset of reconnection in the near magnetotail: PIC simulations. *Journal of Geophysical Research*, *119*, 9773–9789. https://doi.org/10.1002/2014JA020492

Lu, Q. M., Huang, C., Xie, J. L., Wang, R. S., Wu, M. Y., Vaivads, A., & Wang, S. (2010). Features of separatrix regions in magnetic reconnection: Comparison of 2-D particle-in-cell simulations and Cluster observations. *Journal of Geophysical Research*, *115*, A11208. https://doi.org/10.1029/2010JA015713

Lu, Q. M., San, L., Can, H., Mingyu, W., & Wang, S. (2013). Self-reinforcing process of the reconnection electric field in the electron diffusion region and onset of collisionless magnetic reconnection. *Plasma Physics and Controlled Fusion*, *55*, 085019.

Ma, Z. W., & Bhattacharjee, A. (1998). Sudden enhancement and partial disruption of thin current sheets in the magnetotail due to Hall MHD effects. *Geophysical Research Letters*, *25*(17), 3277–3280. https://doi.org/10.1029/98GL02432

Nagai, T., Shinohara, I., Fujimoto, M., Hoshino, M., Saito, Y., Machida, S., & Mukai, T. (2001). Geotail observations of the Hall current system: Evidence of magnetic reconnection in the magnetotail. *Journal of Geophysical Research*, *106*(A11), 25,929–25,949. https://doi.org/10.1029/2001JA900038

Nakamura, R., Baumjohann, W., Asano, Y., Runov, A., Balogh, A., Owen, C. J., et al. (2006). Dynamics of thin current sheets associated with magnetotail reconnection. *Journal of Geophysical Research*, *111*, A11206. https://doi.org/10.1029/2006JA011706

Nakamura, R., Baumjohann, W., Runov, A., & Asano, Y. (2006). Thin current sheets in the magnetotail observed by cluster. *Space Science Reviews*, *122*(1–4), 29–38. https://doi.org/10.1007/s11214-006-6219-1

Ness, N. F. (1965). Earth's magnetic tail. *Journal of Geophysical Research*, *70*(13), 2989–3005. https://doi.org/10.1029/JZ070i013p02989

Petrukovich, A. A., Artemyev, A. V., Malova, H. V., Popov, V. Y., Nakamura, R., & Zelenyi, L. M. (2011). Embedded current sheets in the Earth's magnetotail. *Journal of Geophysical Research*, *116*, A00I25. https://doi.org/10.1029/2010JA015749

Phan, T. D., Eastwood, J. P., Cassak, P. A., Øieroset, M., Gosling, J. T., Gershman, D. J., et al. (2016). MMS observations of electron-scale filamentary currents in the reconnection exhaust and near the X line. *Geophysical Research Letters*, *43*, 6060–6069. https://doi.org/10.1002/2016GL069212

Phan, T. D., Gosling, J. T., Davis, M. S., Skoug, R. M., Øieroset, M., Lin, R. P., et al. (2006). A magnetic reconnection x-line extending more than 390 Earth radii in the solar wind. *Nature*, *439*(7073), 175–178. https://doi.org/10.1038/nature04393

Phan, T. D., Gosling, J. T., Paschmann, G., Pasma, C., Drake, J. F., Oieroset, M., et al. (2010). The dependence of magnetic reconnection on plasma β and magnetic shear: Evidence from solar wind observations. *The Astrophysical Journal*, *719*(2), L199–L203. https://doi.org/10.1088/2041-8205/719/2/L199

Pollock, C., Moore, T., Jacques, A., Burch, J., Gliese, U., Saito, Y., et al. (2016). Fast plasma investigation for Magnetospheric Multiscale. *Space Science Reviews*, *199*(1–4), 331–406. https://doi.org/10.1007/s11214-016-0245-4

Pritchett, P. L., & Coroniti, F. V. (1995). Formation of thin current sheets during plasma sheet convection. *Journal of Geophysical Research*, *100*(A12), 23,551–23,565. https://doi.org/10.1029/95JA02540

Runov, A., Nakamura, R., Baumjohann, W., Zhang, T. L., Volwerk, M., Eichelberger, H. U., & Balogh, A. (2003). Cluster observation of a bifurcated current sheet. *Geophysical Research Letters*, *30*(2), 1036. https://doi.org/10.1029/2002GL016136

Runov, A., Sergeev, V. A., Baumjohann, W., Nakamura, R., Apatenkov, S., Asano, Y., et al. (2005). Electric current and magnetic field geometry in flapping magnetotail current sheets. *Annales de Geophysique*, *23*(4), 1391–1403. https://doi.org/10.5194/angeo-23-1391-2005

Runov, A., Sergeev, V. A., Nakamura, R., Baumjohann, W., Apatenkov, S., Asano, Y., et al. (2006). Local structure of the magnetotail current sheet: 2001 Cluster observations. *Annales de Geophysique*, *24*(1), 247–262. https://doi.org/10.5194/angeo-24-247-2006

Russell, C. T., Anderson, B. J., Baumjohann, W., Bromund, K. R., Dearborn, D., Fischer, D., et al. (2016). The Magnetospheric Multiscale magnetometers. *Space Science Reviews*, *199*(1–4), 189–256. https://doi.org/10.1007/s11214-014-0057-3

Russell, C. T., & Mcpherron, R. L. (1973). Magnetotail and substorms. *Space Science Reviews*, *15*(2–3), 205–266.

Schindler, K., & Birn, J. (2002). Models of two-dimensional embedded thin current sheets from Vlasov theory. *Journal of Geophysical Research*, *107*(A8), 1193. https://doi.org/10.1029/2001JA000304

Schwartz, S. J. (1998). Shock and discontinuity normals, mach numbers, and related parameters. In G. Paschmann & P. W. Daly (Eds.), *Analysis methods for multi spacecraft data* (pp. 249–267). Bern Switzerland: Eur. Space Agency.

Sergeev, V., Runov, A., Baumjohann, W., Nakamura, R., Zhang, T. L., Balogh, A., et al. (2004). Orientation and propagation of current sheet oscillations. *Geophysical Research Letters*, *31*, L05807. https://doi.org/10.1029/2003GL019346

Sergeev, V., Runpov, A., Baumjohann, W., Nakamura, R., Zhang, T. L., Volwerk, M., et al. (2003). Current sheet flapping motion and structure observed by Cluster. *Geophysical Research Letters*, *30*(6), 1327. https://doi.org/10.1029/2002GL016500

Shen, C., Liu, Z. X., Li, X., Dunlop, M., Lucek, E., Rong, Z. J., et al. (2008). Flattened current sheet and its evolution in substorms. *Journal of Geophysical Research*, *113*, A07S21. https://doi.org/10.1029/2007JA012812

Shi, Q. Q., Shen, C., Pu, Z. Y., Dunlop, M. W., Zong, Q. G., Zhang, H., et al. (2005). Dimensional analysis of observed structures using multipoint magnetic field measurements: Application to Cluster. *Geophysical Research Letters*, *32*, L12105. https://doi.org/10.1029/2005GL022454

Sitnov, M. I., Zelenyi, L. M., Malova, H. V., & Slarma, A. S. (2000). Thin current sheet embedded within a thicker plasma sheet: Self-consistent kinetic theory. *Journal of Geophysical Research*, *105*(A6), 13,029–13,043. https://doi.org/10.1029/1999JA000431

Sonnerup, B. U. O. (1979). Magnetic field reconnection. In L. T. Lanzerotti, C. F. Kennel, & E. N. Parker (Eds.), *Solar system plasma physics* (pp. 45–108). New York: North-Holland.

Sonnerup, B. U. Ö., & Scheible, M. (1998). Minimum and maximum variance analysis. In G. Paschmann & P. W. Daly (Eds.), *Analysis methods for multi spacecraft data* (pp. 185–215). Bern, Switzerland: European Space Agency.

Speiser, T. W. (1967). Particle trajectories in model current sheets .2. Applications to auroras ising a geomagnetic tail model. *Journal of Geophysical Research*, *72*(15), 3919.

Terasawa, T. (1983). Hall current effect on tearing mode-instability. *Geophysical Research Letters*, *10*(6), 475–478. https://doi.org/10.1029/GL010i006p00475

Wang, R. S., Lu, Q., Nakamura, R., Huang, C., du, A., Guo, F., et al. (2016). Coalescence of magnetic flux ropes in the ion diffusion region of magnetic reconnection. *Nature Physics*, *12*.

Wang, R. S., Lu, Q. M., Huang, C., & Wang, S. (2010). Multispacecraft observation of electron pitch angle distributions in magnetotail reconnection. *Journal of Geophysical Research*, *115*, A01209. https://doi.org/10.1029/2009JA014553

Wang, R. S., Nakamura, R., Lu, Q., Baumjohann, W., Ergun, R. E., Burch, J. L., et al. (2017). Electron-scale quadrants of the Hall magnetic field observed by the Magnetospheric Multiscale spacecraft during asymmetric reconnection. *Physical Review Letters*, *118*(17).

Wang, R. S., Nakamura, R., Lu, Q., Du, A., Zhang, T., Baumjohann, W., et al. (2012). Asymmetry in the current sheet and secondary magnetic flux ropes during guide field magnetic reconnection. *Journal of Geophysical Research*, *117*, A07223. https://doi.org/10.1029/2011JA017384

Wang, X. G., Bhattacharjee, A., & Ma, Z. W. (2000). Collisionless reconnection: Effects of Hall current and electron pressure gradient. *Journal of Geophysical Research*, *05*, 27,633–27,648.

Zelenyi, L. M., Malova, H. V., Grigorenko, E. E., & Popov, V. Y. (2016). Thin current sheets: From the work of Ginzburg and Syrovatskii to the present day. *Physics-Uspekhi*, *59*(11), 1057–1090. https://doi.org/10.3367/UFNe.2016.09.037923

Zhang, T. L., Baumjohann, W., Nakamura, R., Balogh, A., & Glassmeier, K. H. (2002). A wavy twisted neutral sheet observed by CLUSTER. *Geophysical Research Letters*, *29*(19), 1899. https://doi.org/10.1029/2002GL015544

Zheng, H., Fu, S. Y., Zong, Q. G., Pu, Z. Y., Wang, Y. F., & Parks, G. K. (2012). Observations of ionospheric electron beams in the plasma sheet. *Physical Review Letters*, *109*(20), 205001. https://doi.org/10.1103/PhysRevLett.109.205001